

# Experimental Observation of the Drag Force Suppression in a Flow of Superfluid Light

C. Michel,<sup>1,\*</sup> O. Boughdad,<sup>1</sup> M. Albert,<sup>1</sup> P.É Larré,<sup>2</sup> and M. Bellec<sup>1,†</sup>

<sup>1</sup>Université Côte d'Azur, CNRS, Institut de Physique de Nice, France

<sup>2</sup>Laboratoire Kastler-Brossel, UPMC-Sorbonne Universités, CNRS,

ENS-PSL Research University, Collège de France, 4 Place Jussieu, 75005 Paris, France

We report a direct experimental detection of the frictional-superfluid transition in the flow of a fluid of light past a weakly perturbing localized obstacle in a bulk nonlinear crystal. In our cavityless all-optical system, we extract on the one hand a direct optical analog of the drag force experienced by the obstacle and measure on the other hand the associated obstacle displacement. We observe a superfluid regime characterized by a suppression of long-range radiation from the obstacle, which is, as expected, associated to the cancellation of the drag force and the absence of displacement of the obstacle.

Superfluidity was originally discovered in 1938 [1] when a  $^4\text{He}$  fluid cooled under its  $\lambda$ -point flowed in a nonclassical way along a capillary [2]. This was the trigger for the development of many experiments genuinely realized with quantum matter, as with  $^3\text{He}$  fluids [3] or ultracold atomic vapors [4, 5]. The superfluid behavior of mixed light-matter cavity gases of exciton-polaritons was also extensively studied [6, 7], leading to the emergent field of “quantum fluids of light” [8]. Before being theoretically developed for cavity lasers [9–11], the idea of a superfluid motion of light goes back to pioneering studies in cavityless all-optical configurations (see, e.g., Refs. [12, 13]). In the latter works in particular, the authors studied the hydrodynamic nucleation of quantized vortices past an obstacle when a laser beam propagates in a bulk nonlinear medium. In such a cavityless geometry, in complete analogy with quantum hydrodynamics [4], the paraxial propagation of a monochromatic optical field in a nonlinear medium may be mapped onto a two-dimensional Gross-Pitaevskii-type evolution of a quantum fluid of interacting photons in the plane transverse to the propagation. The intensity, the gradient of the phase and the propagation constant of the optical field serving respectively as the density, the velocity and the mass of the quantum fluid, and the photon-photon interactions being mediated by the optical nonlinearity. It took almost twenty years for this idea to spring up again [14–20], driven by the emergence of advanced laser beam shaping technologies allowing to precisely tailor both the shape of the flow and the potential landscape. This flexibility is unreachable in genuine systems, and will be the basis for the simulation of quantum phase transitions in strongly correlated and/or disordered configurations. From the optics point of view, light superfluidity holds the potential to be a valuable alternative technique for imaging through complex media.

The ways of tracking light superfluidity are manifold. Recently, superfluid hydrodynamics of a fluid of light has been studied in a nonlocal nonlinear liquid through the measurement of the dispersion relation of its elementary excitations [21] and the detection of a vortex nucleation in the wake of an obstacle [22]. The stimulated emission of dispersive shock waves in nonlinear optics was also studied in the context of light superfluidity [14]. However, one of the most striking manifestations of superfluidity — which is the ability of a

fluid to move without friction [23] — has never been directly observed in a cavityless nonlinear-optics platform. A direct consequence of this feature is the absence of long-range radiation in a slow fluid flow past a localized obstacle. In optical terms, this corresponds to the absence of light diffraction from a local modification of the underlying refractive index in the plane transverse to the propagation. In the frictional, non-superfluid regime on the contrary, light becomes sensitive to such an index modification and diffracts while hitting it.

In this Letter, we report a direct experimental detection of the frictional-superfluid transition in the flow of a fluid of light past a weakly perturbing localized obstacle in a bulk nonlinear crystal. As a matter of fact, we observe a superfluid regime characterized by an absence of long-range radiation from the obstacle. This regime is usually associated to the cancellation of the drag force experienced by the obstacle, as studied for  $^4\text{He}$  [24], ultracold atomic vapors [25–30], or cavity exciton-polaritons [31–33]. In our cavityless all-optical system, we extract on the one hand a quantity corresponding to the optical analog of this force and measure on the other hand the associated obstacle displacement. For the first time, we observe that this displacement is nonzero in the nonsuperfluid regime and tends to vanish while reaching the superfluid regime.

We make use of a biased photorefractive crystal which is a perfect candidate, thanks to its controllable nonlinear optical response, for probing the hydrodynamic behavior of light [14, 34]. As sketched in Fig. 1.a and detailed below, a local drop of the optical index is photo-induced by a narrow beam in the crystal and creates the obstacle (green beam, denoted with subscript “ob” in Fig. 1.c). Simultaneously, a second, larger monochromatic beam is sent into the crystal and creates the fluid of light (red beam, denoted with subscript “f” in Fig. 1.c). The propagation of the fluid of light beam in the paraxial approximation (see, e.g., [35]) is ruled by the two-dimensional Gross-Pitaevskii-type equation (also known as the nonlinear Schrödinger equation):

$$i\partial_z E_f = -\frac{1}{2n_e k_f} \nabla^2 E_f - k_f \Delta n(I_{\text{ob}}) E_f - k_f \Delta n(I_f) E_f \quad (1)$$

Here, the propagation coordinate  $z$  plays the role of time. The transverse-plane coordinates  $\mathbf{r} = (x, y)$  span the two-dimensional space in which the fluid of light evolves. The propagation constant  $n_e k_f$  of the fluid of light beam (with

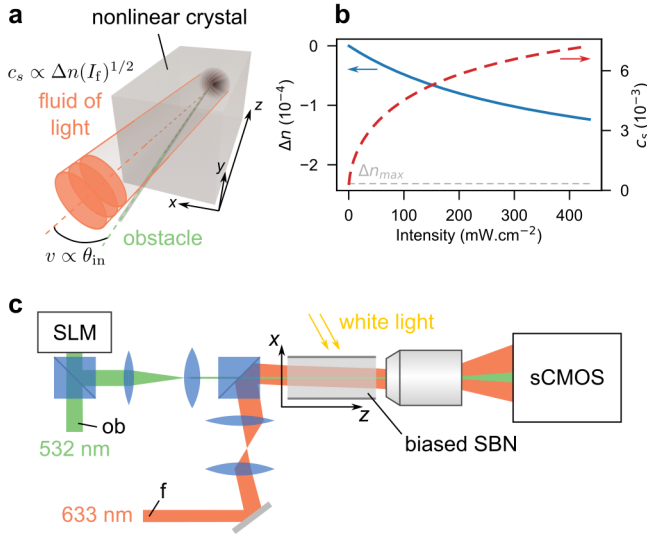


FIG. 1. (Color online) **a.** Sketch of the fluid of light (red beam) flowing past a localized obstacle (green beam). The velocity  $v$  of the fluid of light is proportional to the input angle  $\theta_{\text{in}}$ . The speed of sound  $c_s$  (the critical velocity for superfluidity in the weakly perturbing regime) depends on the unperturbed intensity  $I_f$  of the red beam. **b.** *Blue curve.* Calculated optical-index variation  $\Delta n$  with respect to a laser intensity  $I$  for  $\Delta n_{\text{max}} = -2.32 \times 10^{-4}$ , the theoretical limit expected for the photorefractive response of the medium and  $I_{\text{sat}} = 380 \text{ mW} \cdot \text{cm}^{-2}$ , the saturation intensity extracted from experimental measurements (see Fig. 4). *Red dashed curve.* Corresponding superfluid critical velocity  $c_s$ . The velocity  $v$  of the fluid of light varies from 0 to  $\pm 1.3 \times 10^{-2}$ . **c.** Experimental setup. The green beam is shaped by the spatial light modulator (SLM) to create a  $z$ -invariant optical defect acting as a localized obstacle in the transverse plane. The red beam is a large gaussian beam and creates the fluid of light. Both are propagating simultaneously through a biased SBN photorefractive crystal. The near-field intensity is imaged on a sCMOS camera.

$k_f = 2\pi/\lambda_f$  its free-space counterpart and  $n_e$  the crystal's refractive index) plays the role of a mass and the associated Laplacian term  $\nabla^2 = \partial_{xx} + \partial_{yy}$  describes light diffraction in the transverse plane. The intensity  $I_f \propto |E_f|^2$  and the gradient of the phase of the complex envelope  $E_f$  of the electric field  $\text{Re}(E_f e^{in_e k_f z})$  respectively play the role of the density and the velocity  $v = (n_e k_f)^{-1} |\partial \arg(E_f)/\partial \mathbf{r}|$  of the fluid of light. The local refractive-index depletion  $\Delta n[I_{\text{ob}}(\mathbf{r})] < 0$  induced by the obstacle beam of intensity  $I_{\text{ob}}(\mathbf{r})$  corresponds to a repulsive potential. The self-defocusing nonlinear contribution  $\Delta n(I_f) < 0$  to the total refractive index provides repulsive photon-photon interactions and ensures robustness against modulational instabilities [36]. From the latter, we define a healing length  $\xi = [n_e k_f \times k_f |\Delta n(I_f)]^{-1/2}$  which corresponds to the smallest length scale for intensity modulations. We define as well a critical speed  $c_s = (n_e k_f \times \xi)^{-1} = [|\Delta n(I_f)|/n_e]^{1/2}$  for the fluid of light, historically called a speed of sound [4, 20]. Both quantities directly depend on the intensity  $I_f$  of the fluid of light beam which is here evaluated far away from the obstacle where the fluid of light remains

unperturbed. Although analogously referred to a speed, note that  $c_s$  is here dimensionless, as  $v$  defined above.

When the obstacle is weakly perturbing, Landau's criterion for superfluidity [23] applies and the so-called Mach number  $v/c_s$  mediates the transition from a nonsuperfluid regime at large  $v/c_s$  to a superfluid regime at low  $v/c_s$ . The speed of sound then corresponds to the critical velocity for superfluidity. In the experiment, the fluid of light beam consists in a gaussian beam which is large compared to the size of the obstacle (see Fig. 1.a). It can be approximated by a plane wave whose phase  $\mathbf{k}_{\perp} \cdot \mathbf{r}$  remains constant in the vicinity of the obstacle, with  $k_{\perp} = k_f \sin \theta_{\text{in}}$  the transverse wave vector of the plane wave. Consequently,  $v$  is only given by  $\theta_{\text{in}}$ , the angle between the fluid of light beam and the  $z$  direction:  $v = \sin \theta_{\text{in}}/n_e \simeq \theta_{\text{in}}/n_e$  in the here-considered paraxial approximation. The ratio  $v/c_s$  is thus controlled by the incidence angle  $\theta_{\text{in}}$  and/or by the unperturbed intensity  $I_f$  of the fluid of light beam. Note, however, that these two ways of tuning the Mach number are not exactly equivalent since changing the intensity also affects other quantities like the healing length and the relative strength of the obstacle with respect to the nonlinear term.

The experimental setup is presented in Fig. 1.c. The nonlinear medium consists in a  $5 \times 5 \times 10 \text{ mm}^3$  strontium barium niobate (SBN:61) photorefractive crystal additionally doped with cerium (0.01%) to enhance its photoconductivity [37] albeit it induces some linear absorption that we shall discuss later on while interpreting our experimental results. The basic mechanism of the photorefractive effect remains in the photogeneration and displacement of mobile charge carriers driven by an external electric field  $E_0$ . The induced permanent space-charge electric field thus implies a modulation of the refractive index of the crystal [38, 39],  $\Delta n(I, \mathbf{r}) = -0.5n_e^3 r_{33} E_0 / [1 + I(\mathbf{r})/I_{\text{sat}}]$ , where  $n_e$  is the optical index and  $r_{33}$  the electro-optic coefficient of the material along the extraordinary axis,  $I(\mathbf{r})$  is the intensity of the optical beam in the transverse plane  $\mathbf{r}(x, y)$ , and  $I_{\text{sat}}$  is the saturation intensity which can be adjusted with a white light illumination of the crystal. The blue curve in Fig. 1.b shows the saturable nonlinear response of the material  $\Delta n(I)$  versus a laser intensity  $I$ . The red dashed curve represents as for it the superfluid critical velocity  $c_s(I)$  for the saturable nonlinear response of the material  $\Delta n(I)$ . The saturation intensity  $I_{\text{sat}} = 380 \text{ mW} \cdot \text{cm}^{-2}$  used in the calculations is extracted from experimental measurements (see Fig. 4). The maximum value of the optical index variation is theoretically  $\Delta n_{\text{max}} = -2.32 \times 10^{-4}$  for  $E_0 = 1.5 \text{ kV} \cdot \text{cm}^{-1}$ .

Making use of a spatial light modulator, we produce a diffraction-free Bessel beam ( $\lambda_{\text{ob}} = 532 \text{ nm}$ ,  $I_{\text{ob}} = 7.6 \text{ W} \cdot \text{cm}^{-2} \gg I_{\text{sat}}$ , green path in Fig. 1.c). The latter creates the obstacle with a radius of  $6 \mu\text{m}$  (comparable to  $\xi = 6.2 \mu\text{m}$  for  $I_f = 349 \text{ mW} \cdot \text{cm}^{-2}$ ) that is constant all along the crystal and aligned with the  $z$ -direction. From Fig. 1.b, the propagation of the obstacle beam into the crystal induces a local drop  $\Delta n(I_{\text{ob}}) = -2.2 \times 10^{-4}$  in the refractive index. A second laser ( $\lambda_f = 633 \text{ nm}$ , red path in Fig. 1.c) delivers a gaussian

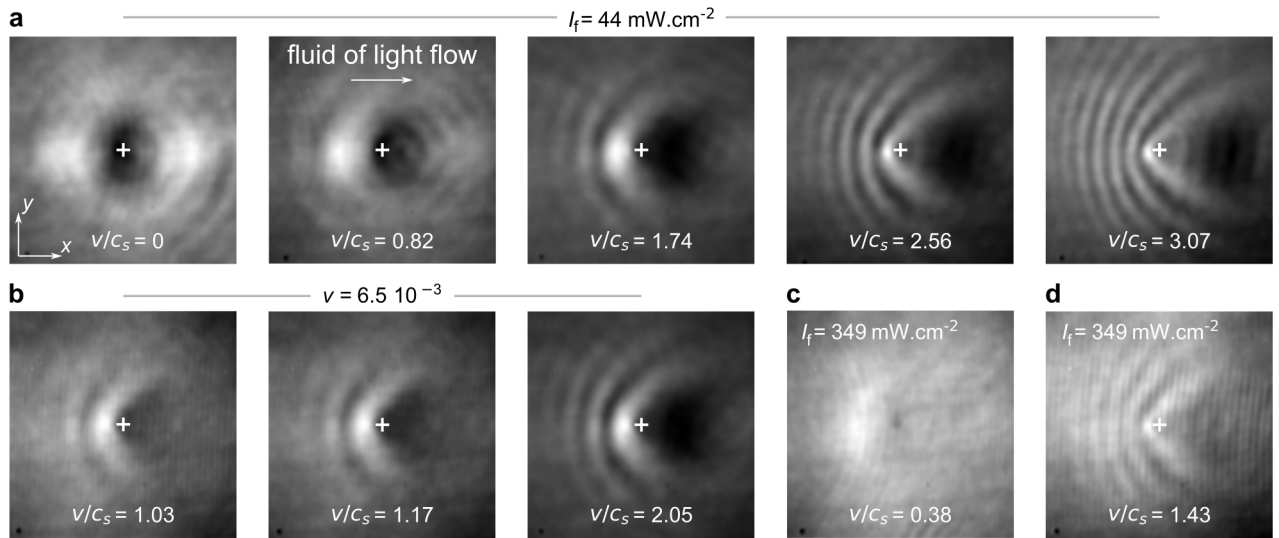


FIG. 2. (Color online) Spatial distribution of the output intensity of the fluid of light for various input conditions. The white crosses (arrow) indicate(s) the central position of the obstacle (the direction of the flow). Each image is  $330 \times 330 \mu\text{m}^2$ . **a.** At a fixed input intensity,  $I_f = 44 \text{ mW} \cdot \text{cm}^{-2}$  (corresponding to the speed of sound  $c_s = 3.2 \times 10^{-3}$ ), the input angle  $\theta_{\text{in}}$  of the beam creating the fluid of light varies from 0 to 23 mrad (corresponding to a flow velocity  $v$  varying from 0 to  $9.8 \times 10^{-3}$ ). Accordingly, the Mach number  $v/c_s$  varies from 0 to 3.07. **b.** At a fixed  $\theta_{\text{in}} = 15.3 \text{ mrad}$  ( $v = 6.5 \times 10^{-3}$ ),  $I_f$  varies from 44 to 262  $\text{mW} \cdot \text{cm}^{-2}$  ( $c_s$  varies from  $3.2 \times 10^{-3}$  to  $6.3 \times 10^{-3}$ ). Accordingly,  $v/c_s$  varies from 1.03 to 2.05. **c.** For  $I_f = 349 \text{ mW} \cdot \text{cm}^{-2}$  ( $c_s = 6.8 \times 10^{-3}$ ) and  $\theta_{\text{in}} = 6.1 \text{ mrad}$  ( $v = 2.6 \times 10^{-3}$ ), which corresponds to  $v/c_s = 0.38$ , the fluid of light is in the superfluid regime. The remaining lack of uniformity upstream from the obstacle is attributed to propagation losses due to linear absorption. **d.** For  $I_f = 349 \text{ mW} \cdot \text{cm}^{-2}$  ( $c_s = 6.8 \times 10^{-3}$ ) and  $\theta_{\text{in}} = 23.1 \text{ mrad}$  ( $v = 9.8 \times 10^{-3}$ ), which corresponds to  $v/c_s = 1.43$ , the fluid of light is in a Čerenkov, nonsuperfluid regime.

beam whose radius is extended to  $270 \mu\text{m}$  and which corresponds to the fluid of light beam. As already mentioned, we vary the flow velocity  $v$  by changing the input angle  $\theta_{\text{in}}$  of the fluid of light beam with respect to the propagation axis along the crystal (see Fig. 1.a). The accessible range goes from  $v = 0$  to  $v = \pm 1.3 \times 10^{-2}$ . The critical velocity  $c_s$  for superfluidity is controlled by the input intensity of the beam which can be tuned from  $I_f = 0$  to  $350 \text{ mW} \cdot \text{cm}^{-2}$ . For the detection part, a  $20\times$  microscope objective and a sCMOS camera allow to get the spatial distribution of the near-field intensity of the beams at the output of the crystal.

Depending on the width and the depth of the obstacle, different regimes can be explored [20]. In the present paper, we limit our study to the case of a weakly perturbing obstacle (weak  $\Delta n[I_{\text{ob}}(\mathbf{r})]$  and radius of the order of  $\xi$ ) for which the transition from a frictional to a superfluid motion is expected not to be blurred by the emission of nonlinear excitations like vortex pairs, oblique solitons, etc. Figure 2 presents typical experimental results for the spatial distribution of the light intensity observed at the output of the crystal for various input conditions. Figure 2.a displays the output spatial distribution of the light intensity for different fluid velocities  $v$  (i.e., input angles  $\theta_{\text{in}}$ ) at a fixed speed of sound,  $c_s = 9.9 \times 10^{-3}$  (obtained for  $I_f = 44 \text{ mW} \cdot \text{cm}^{-2}$ ). This allows to vary  $v/c_s$  from 0 to 3.1. As expected, for  $v = 0$ , one sees no diffraction but just the optical defect in which light is not guided. As  $v$  increases, diffraction appears in the transverse plane, and progressively manifests as a characteristic cone of fringes up-

stream from the obstacle (see Fig. 2.a). Another way to probe the transition is to fix the transverse velocity  $v$  and to vary the critical velocity  $c_s$  through the variation of the intensity of the fluid of light beam. As shown in Fig. 2.b, the results are similar with the interference pattern becoming more and more pronounced as  $v/c_s$  increases. Figure 2.d represents a situation for which  $v/c_s = 1.43$ . In this case, a Mach-Čerenkov cone is clearly visible upstream from the obstacle [16, 20, 40]. In the subsonic,  $v/c_s \ll 1$ , regime, diffraction is expected to disappear, meaning that the fluid of light flows around the obstacle in a superfluid way. Figure 2.c represents the intensity distribution at the output of the crystal for  $v/c_s = 0.38$  ( $I_f = 349 \text{ mW} \cdot \text{cm}^{-2}$ ). As expected, long-range radiation upstream from the obstacle is no longer present in this case, indicating a superfluid motion of light. Note that the lack of uniformity of the intensity upstream from the obstacle is due to the intrinsic linear absorption of the material. For a deeper obstacle (strong  $\Delta n[I_{\text{ob}}(\mathbf{r})]$  and/or radius  $\gg \xi$ ), a transient regime should be observed with a more complex dynamics involving the typical generation of vortex alleys or oblique solitons [22, 41]. This regime will be subjected to a further study.

In the supersonic ( $v/c_s > 1$ ), frictional regime, the intensity modulation of the fluid of light flowing around the obstacle induces a local optical index modification of the material. This modification influences the propagation of the beam responsible for the obstacle, for which a transverse displacement is expected. On the contrary, in the subsonic ( $v/c_s \ll 1$ ), superfluid regime, the absence of intensity modulation implies

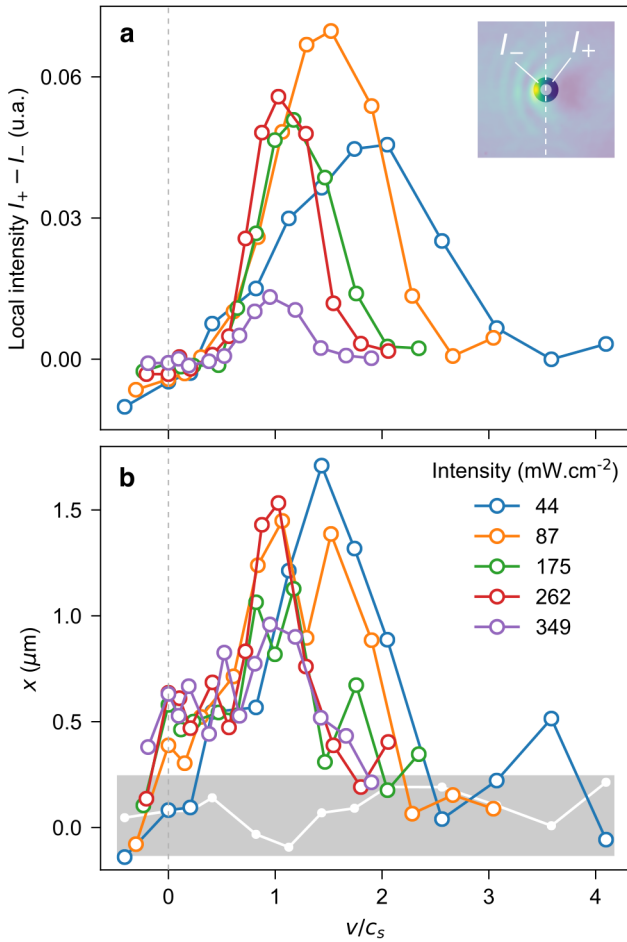


FIG. 3. (Color online) **a**. Local intensity difference  $I_+ - I_-$  extracted from the experimental images of the intensity of the fluid of light beam measured at the crystal's output for various input conditions ( $I_f$  ranging from 44 to 349  $\text{mW}\cdot\text{cm}^{-2}$  and  $v/c_s$  ranging from -0.41 to 4.10). The inset illustrates the data processing. The original image is cropped around the optical defect and integrated in two regions, downstream ( $I_-$ ) and upstream ( $I_+$ ). The typical integration area is of the order of  $\xi$ . The gray dotted line corresponds to  $v/c_s = 0$ . **b**. Measurement of the transverse displacement of the obstacle induced by the local modulation of the intensity of the fluid of light for various input conditions. The gray box defines the typical uncertainty in the measured quantities, the white points corresponding to the displacement along the  $y$  axis for  $I_f = 44 \text{ mW}\cdot\text{cm}^{-2}$ , which is expected to be zero.

no local variation of the optical index and then one does not wait for any displacement of the obstacle beam. In the following, we first extract the local intensity difference for the fluid of light between the front ( $I_+$ ) and the back ( $I_-$ ) of the obstacle at the output of the crystal. As investigated in [42] for a material obstacle (here, we rather consider here an all-optical obstacle),  $I_+ - I_-$  is proportional to the dielectric force experienced by the obstacle, and this force turns out to be closely analogous to the drag force that a flowing atomic dilute Bose quantum fluid may exert onto an obstacle. While the drop of this force is among the main signatures of superfluid-

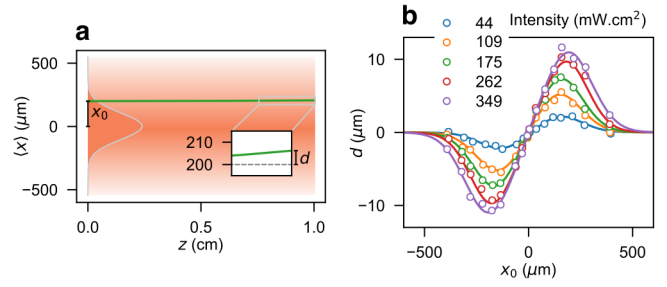


FIG. 4. (Color online) Transverse displacement of the obstacle in a gaussian potential. **a**. Calculated transverse displacement  $\langle x \rangle$  along the propagation,  $z$ , axis for a potential induced by a  $270 \mu\text{m}$  at  $1/e^2$  half-width gaussian laser beam of intensity  $I_f = 175 \text{ mW}\cdot\text{cm}^{-2}$ .  $x_0 = 200 \mu\text{m}$  is the initial position of the obstacle.  $d$  is the transverse displacement, with respect to  $x_0$ , at the crystal's output. **b**. Measured transverse displacement for various laser beam intensities  $I_f$  ranging from 44 to 349  $\text{mW}\cdot\text{cm}^{-2}$  as a function of  $x_0$ . The fit procedure (solid lines) allows to extracted  $I_{\text{sat}} = 380 \pm 50 \text{ W}\cdot\text{cm}^{-2}$  and  $\Delta n_{\text{max}} = 2.5 \pm 0.4 \times 10^{-4}$ .

ity in material fluids, so far no experiments on fluids of light have proposed to investigate it. Figure 3.a depicts the variation of  $I_+ - I_-$  as a function of  $v/c_s$  for various initial conditions ( $I_f$  varies from 44 to 349  $\text{mW}\cdot\text{cm}^{-2}$  and  $v/c_s$  ranges from -0.41 to 4.10). As illustrated in the inset, both intensities are integrated over a typical distance of the order of  $\xi$  surrounding the obstacle. We observe a rather smooth, but net transition around  $v/c_s = 1$ . For low  $v/c_s < 1$  and large  $I_f$ , we fall into the superfluid regime and the signal vanishes. The increasing tendency for low Mach numbers is associated to linear absorption (of the order of 3.2 dB/cm), as discussed in the context of cavity quantum fluids of light [31, 32, 43]. The well-known decreasing tendency at large Mach numbers is here also observed. Indeed, the obstacle can always be treated as a perturbation at large velocities and the associated drag force resultingly decreases (the large-velocity limit was accordingly denoted as “quasiideal” in [44]). Moreover, Fig. 3.a shows that the curves with different intensity  $I_f$ , although renormalized by the respective sound velocity  $c_s$ , do not fall on a single universal curve. As mentioned previously, this is due to the fact that changing the intensity also affects crucial quantities like the healing length  $\xi$  and the relative strength of the obstacle with respect to the nonlinear term,  $\Delta n(I_{\text{ob}})/\Delta n(I_f)$ .

We then propose to probe the corresponding presence/absence of transverse displacement for the obstacle, independently on the measurement of  $I_+ - I_-$ . As a first step, we calibrate the displacement considering the linear propagation of the green beam creating the obstacle in the optical potential  $\Delta n(I_f)$  photo-induced by the fluid of light beam. In the here-considered paraxial approximation, the propagation equation reads:

$$i\partial_z E_{\text{ob}} = -\frac{1}{2n_e k_{\text{ob}}} \nabla^2 E_{\text{ob}} - k_{\text{ob}} \Delta n(I_f) E_{\text{ob}} \quad (2)$$

with trivial notations; see Eq. (1). By assuming that the transverse component of the fluid of light beam is non-zero only

along the  $x$  axis, we denote by  $\langle x \rangle = \int x |E_{\text{ob}}|^2 dx$  the position of the centroid of the obstacle beam. Using an optical equivalent of the Ehrenfest theorem, one can derive from eq.(2) the following equation of motion:  $(n_e k_{\text{ob}}) \partial_{zz} \langle x \rangle = -\partial_x [-k_{\text{ob}} \Delta n(I_f)]$ . We assume that  $\Delta n$  is  $z$  independent, which is valid in the here-considered linear propagation of the obstacle beam. We readily obtain  $\langle x(z) \rangle - x_0 = \frac{1}{2} [\partial_x \Delta n(I_f) / n_e] z^2$  where  $x_0$  is the initial position of the obstacle. This displacement is interpreted as the consequence of a force deriving from the optical potential  $-k_{\text{ob}} \Delta n(I_f)$ , and acting on the obstacle. As shown in Fig. 4.a, for  $x_0 = 200 \mu\text{m}$  and an optical potential induced by a  $270 \mu\text{m}$  wide gaussian beam of intensity  $I_f = 175 \text{ mW.cm}^{-2}$ , the relative transverse displacement  $d = \langle x(L) \rangle - x_0$  reaches  $7.8 \mu\text{m}$  at the output of the crystal (see inset). The experimental measurement of  $d$ , for various intensities and positions  $x_0$ , is presented in Fig. 4.b. The experimental data are fitted (solid lines), using the above expression, the saturation intensity and the maximum refractive index modification being the fitting parameters. We extract  $I_{\text{sat}} = 380 \pm 50 \text{ mW.cm}^{-2}$  and  $\Delta n_{\text{max}} = 2.5 \pm 0.4 \times 10^{-4}$ . It is worth mentioning that the value of  $I_{\text{sat}}$  is used for the calculation of  $\Delta n(I)$  and its deriving quantities (i.e.,  $c_s$  and  $\xi$ ).

We clearly observe that the all-optical obstacle is highly sensitive to the surrounding refractive index potential resulting from the spatial distribution of intensity of the beam creating the fluid of light. The next step is to probe the transition from the frictional to the superfluid regimes by detecting the evolution of its transverse displacement while varying the Mach number  $v/c_s$ . To this end, we measure the displacement for various input conditions for the fluid of light. For each data point, we subtract the displacement measured at very low obstacle intensity (i.e. when its influence on the fluid of light is negligible). The result is shown in Fig. 3.b. Note that the displacement along the  $y$  direction, measured for  $I_f = 44 \text{ mW.cm}^{-2}$  and which is expected to be zero, is represented by the white data and allows us to define the typical measurement uncertainty for this experiment (gray box). The fluctuation can be attributed to the inherent imperfections of the fluid of light beam. As expected, the transverse displacement of the obstacle behaves very similarly to the intensity difference  $I_+ - I_-$  displayed in Fig. 3.a. That is, an increasing displacement from almost zero (in the subsonic, superfluid regime  $v/c_s \ll 1$ ) to maximum signal (around  $v/c_s = 1$ ) and a decreasing signal in the supersonic, nonsuperfluid regime  $v/c_s > 1$ . We also measured an opposite transverse displacement for negative  $v/c_s$ . The fact that the displacement is not purely zero in the superfluid regime is likely due to the displacement acquired during the non-stationary regime at early stage of the propagation. This is, to the best of our knowledge, the first observation of the displacement of an all-optical obstacle in a fluid of light.

To conclude, we reported a direct experimental observation of the transition from a frictional to a superfluid regimes in a cavityless all-optical propagating geometry. We performed a quantitative study by extracting an optical equivalent of the

drag force that the fluid of light exerts on the obstacle. This result is in very good agreement with a second, independent, measurement that consists in studying the spatial displacement of the obstacle surrounded by a the fluid of light. We restricted the present study to the case of a weakly perturbing obstacle but our experimental apparatus allows to reach the turbulent regime associated to vortex generation through the induction of a greater optical index depletion. On the other hand, a different shaping of the beam creating the obstacle will allow to generate any kind of optical potential and to extend the study to imaging through disordered environments.

We thank I. Carusotto for helpful discussions. This work has been supported by the the Region PACA and the French government, through the UCA<sup>IEDI</sup> Investments in the Future project managed by the National Research Agency (ANR) with the reference number ANR-15-IDEX-01. P.-É. L. was funded by the Centre National de la Recherche Scientifique (CNRS) and by the ANR under the grant ANR-14-CE26-0032 LOVE.

\* [claire.michel@unice.fr](mailto:claire.michel@unice.fr)

† [bellec@unice.fr](mailto:bellec@unice.fr)

- [1] P. Kapitza, Nature **141**, 74 (1938).
- [2] J. F. Allen and A. D. Misener, Nature **141**, 75 (1938).
- [3] D. D. Osheroff, R. C. Richardson, and D. M. Lee, Phys. Rev. Lett. **28**, 885 (1972).
- [4] L. Pitaevskii and S. Stringari, *Bose-Einstein Condensation and Superfluidity* (Oxford University Press, 2016).
- [5] I. Bloch, J. Dalibard, and S. Nascimbène, Nat. Phys. **8**, 267 (2012).
- [6] A. Amo, J. Lefrère, S. Pigeon, C. Adrados, C. Ciuti, I. Carusotto, R. Houdré, E. Giacobino, and A. Bramati, Nat. Phys. **5**, 11 (2009).
- [7] A. Amo, S. Pigeon, D. Sanvitto, V. Sala, R. Hivet, I. Carusotto, F. Pisanello, G. Leménager, R. Houdré, E. Giacobino, C. Ciuti, and A. Bramati, Science **332**, 6034 (2011).
- [8] I. Carusotto and C. Ciuti, Rev. Mod. Phys. **85**, 299 (2013).
- [9] M. Vaupel, K. Staliunas, and C. O. Weiss, Phys. Rev. A **80**, 880 (1996).
- [10] R. Y. Chiao and J. Boyce, Phys. Rev. A **60**, 4114 (1999).
- [11] E. L. Bolda, R. Y. Chiao, and W. H. Zurek, Phys. Rev. Lett. **86**, 416 (2001).
- [12] T. Frisch, Y. Pomeau, and S. Rica, Phys. Rev. Lett. **69**, 11 (1992).
- [13] Y. Pomeau and S. Rica, C. R. Acad. Sci. Paris **397**, 1287 (1993).
- [14] W. Wan, S. Jia, and J. W. Fleischer, Nat. Phys. **3**, 46 (2007).
- [15] S. Jia, W. Wan, and J. W. Fleischer, Phys. Rev. Lett. **99**, 223901 (2007).
- [16] E. G. Khamis, A. Gammal, G. A. El, Y. G. Gladush, and A. M. Kamchatnov, Phys. Rev. A **78**, 013829 (2008).
- [17] W. Wan, D. V. Dylov, C. Barsi, and J. W. Fleischer, Opt. Lett. **35**, 16 (2010).
- [18] P. Leboeuf and S. Moulieras, Phys. Rev. Lett. **105**, 163904 (2010).
- [19] S. Jia, M. Haataja, and J. W. Fleischer, New J. Phys. **14**, 075009 (2012).
- [20] I. Carusotto, Proc. R. Soc. A **470**, 0320 (2014).
- [21] D. Vocke, T. Roger, F. Marino, E. M. Wright, I. Carusotto,

- M. Clerici, and D. Faccio, *Optica* **2** (2015).
- [22] D. Vocke, K. Wilson, F. Marino, I. Carusotto, E. M. Wright, T. Roger, B. P. Anderson, P. Öhberg, and D. Faccio, *Phys. Rev. A* **94**, 013849 (2016).
- [23] A. Leggett, *Rev. Mod. Phys.* **71**, S318 LP (1999).
- [24] D. R. Allum, P. V. E. McWintock, A. Phillips, and R. M. Bowley, *Philosophical Transactions of the Royal Society of London A* **284**, 179 (1977).
- [25] C. Raman, M. Kohl, R. Onofrio, D. S. Durfee, C. E. Kulewicz, Z. Hadzibabic, and W. Ketterle, *Phys. Rev. Lett.* **83**, 2502 (1999).
- [26] R. Onofrio, C. Raman, J. M. Vogels, J. R. Abo-Shaeer, A. P. Chikkatur, and W. Ketterle, *Phys. Rev. Lett.* **85**, 2228 (2000).
- [27] N. Pavloff, *Phys. Rev. A* **66**, 013610 (2002).
- [28] D. E. Miller, J. K. Chin, C. A. Stan, Y. Liu, W. Setiawan, C. Sanner, and W. Ketterle, *Phys. Rev. Lett.* **99**, 070402 (2007).
- [29] P. Engels and C. Atherton, *Phys. Rev. Lett.* **99**, 160405 (2007).
- [30] R. Desbuquois, L. Chomaz, T. Yefsah, J. Léonard, J. Beugnon, C. Weitenberg, and J. Dalibard, *Nat. Phys.* **8**, 645 (2012).
- [31] M. Wouters and I. Carusotto, *Phys. Rev. Lett.* **105**, 020602 (2010).
- [32] A. C. Berceanu, E. Cancellieri, and F. M. Marchetti, *J. Phys.: Condens. Matter* **24**, 235802 (2012).
- [33] M. Van Regemortel and M. Wouters, *Phys. Rev. B* **89**, 085303 (2014).
- [34] C. Sun, S. Jia, C. Barsi, S. Rica, A. Picozzi, and J. W. Fleischer, *Nat. Phys.* **8**, 470 (2012).
- [35] R. Boyd, *Nonlinear Optics 3<sup>rd</sup> Edition* (Academic Press, 2008).
- [36] P. E. Larré, S. Biasi, F. Ramiro-Manzano, L. Pavesi, and I. Carusotto, *Eur. Phys. J. D* **71**, 146 (2017).
- [37] K. Buse, *Appl. Phys. B* **64**, 391 (1997).
- [38] C. Denz, M. Schwab, and C. Weillau, *Transverse-Pattern Formation in Photorefractive Optics* (Springer-Verlag, Berlin, 2003).
- [39] R. Allio, D. Guzmán-Silva, C. Cantillano, L. Morales-Inostroza, D. Lopez-Gonzalez, S. Etcheverry, R. Vicencio, and J. Armijo, *J. Opt.* **17**, 025101 (2014).
- [40] I. Carusotto, S. X. Hu, L. A. Collins, and A. Smerzi, *Phys. Rev. Lett.* **97**, 260403 (2006).
- [41] G. Nardin, G. Grosso, Y. Lger, B. Pietka, F. Morier-Genoud, and B. Deveaud-Pldran, *Nat. Phys.* **7**, 8 (2011).
- [42] P.-É. Larré and I. Carusotto, *Phys. Rev. A* **91**, 053809 (2015).
- [43] P.-É. Larré, N. Pavloff, and A. Kamchatnov, *Phys. Rev. B* **86**, 165304 (2012).
- [44] M. Albert, T. Paul, N. Pavloff, and P. Leboeuf, *Phys. Rev. Lett.* **100**, 250405 (2008).